JACS
JOURNAL OF THE AMERICAN CHEMICAL SOCIETY
Article
pubs.acs.org/JACS

Dimer Involvement and Origin of Crossover in Nickel-Catalyzed Aldehyde−Alkyne Reductive Couplings

M. Taylor Haynes II,[†,§] Peng Liu,[‡,§,∥] Ryan D. Baxter,[†,⊥] Alex J. Nett,[†] K. N. Houk,*[,‡] and John Montgomery*[,†]

[†]Department of Chemistry, University of Michigan, 930 North University Avenue, Ann Arbor, Michigan 48109-1055, United States
[‡]Department of Chemistry and Biochemistry, University of California, Los Angeles, California 90095-1569, United States

Supporting Information

ABSTRACT: The mechanism of nickel(0)-catalyzed reductive coupling of aldehydes and alkynes has been studied. Extensive double-labeling crossover studies have been conducted. While previous studies illustrated that phosphine- and *N*-heterocyclic carbene-derived catalysts exhibited differing behavior, the origin of these effects has now been evaluated in detail. Many variables, including ligand class, sterics of the ligand and alkyne, temperature, and ring size being formed in intramolecular versions, all influence the extent of crossover observed. A computational evaluation of these effects suggests that dimerization of a key metallacyclic intermediate provides the origin of crossover. Protocols that proceed with crossover are typically less efficient than those without crossover given the thermodynamic stability and low reactivity of the dimeric metallacycles involved in crossover pathways.

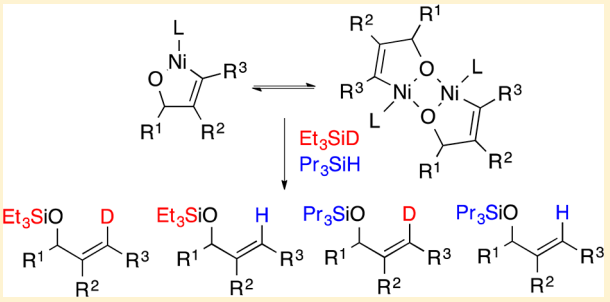

INTRODUCTION

The nickel-catalyzed reductive coupling of aldehydes with alkynes has been widely studied in both intra- and intermolecular forms across a broad range of substrates, reducing agents, and ligands.[1,2] Numerous reports employing organozinc,[3] organoborane,[4] and organosilane[5] reducing agents with phosphine and *N*-heterocyclic carbene (NHC) ligands have appeared. In the first report of nickel-catalyzed aldehyde−alkyne reductive couplings, the reductive cyclization of an ynal was demonstrated employing phosphine ligands and diethylzinc as the reducing agent.[3a] In that report, the generation of a metallacyclic intermediate derived from oxidative cyclization of Ni(0) with the ynal substrate, followed by conversion of the metallacycle to product by a transmetalation/β-hydride elimination/reductive elimination sequence, was proposed. Many subsequent developments in nickel-catalyzed reductive couplings of aldehydes and alkynes have suggested related mechanistic pathways involving metallacyclic intermediates, followed by a late-stage involvement of the reducing agent. More recent developments described procedures of broader scope involving different reducing agent and ligand combinations, such as the use of Et_3B-mediated couplings with phosphine ligands from Jamison[4] and the use of silanes with *N*-heterocyclic carbene ligands from our laboratories.[5c,d] These improved methods allow for challenging intermolecular couplings[6] and macrocyclizations,[7] whereas the prior advances were largely limited to five- and six-membered ring cyclizations. The pathway for the generally proposed mechanism involving silane reducing agents, which is the focus of this study, is depicted in Scheme 1.

Scheme 1. Commonly Proposed Metallacycle Pathway

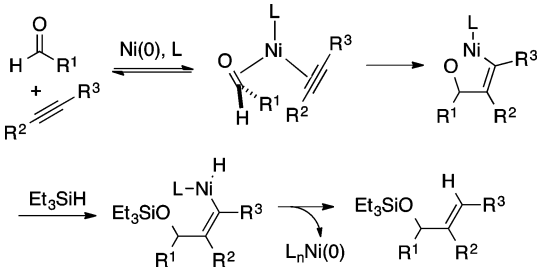

Key pieces of data have largely supported the metallacycle mechanism in reactions of this type. Stoichiometric generation of the metallacycle derived from $Ni(COD)_2$, PCy_3, benzaldehyde, and butyne was described by Ogoshi (Scheme 2).[8] In this case, a dimeric form of the metallacycle was characterized by crystallographic analysis, although no implications of metallacycle aggregation have been suggested as a significant

Scheme 2. Ogoshi's Metallacycle Dimer

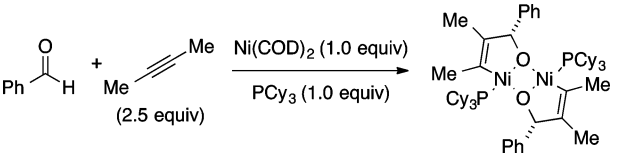

Received: August 28, 2014
Published: November 17, 2014

   dx.doi.org/10.1021/ja508909u | J. Am. Chem. Soc. 2014, 136, 17495−17504

mechanistic feature. Computational studies have provided considerable insight into processes of this type, including studies of intermolecular couplings employing phosphine ligands and organoborane reducing agents as well as the use of NHC ligands and organosilane reducing agents.[9] In both cases, the formation of a metallacycle, followed by subsequent reduction, was found to be the operative pathway among several proposed reactive pathways. Recent experimental work included an initial rates analysis of intramolecular ynal reductive couplings employing PCy_3 as the ligand with triethylsilane as the reducing agent.[10] In that study, the reaction was found to be first order in both ynal and nickel and zeroth order in silane. Additionally, the report included an in situ IR study, which showed that direct addition of the silane to the nickel phosphine catalyst does not occur on the time scale of catalytic reactions unless both the aldehyde and alkyne are present.[11] All of the above studies, across a broad range of ligands and reducing agents, are unified in the conclusion that aldehyde–alkyne reductive couplings proceed through a metallacycle intermediate before reduction to the corresponding silyl-protected allylic alcohols.

Prior to much of the above mechanistic insight being obtained, Montgomery reported in 2004 that the silane-mediated reductive couplings of aldehydes and alkynes using NHC ligands showed a substantial increase in scope in comparison to the earlier reported silane-mediated phosphine-promoted variant.[5c] In that study, a series of crossover experiments were described, employing a mixture of Et_3SiD and Pr_3SiH. Studies of this type are exceptionally useful in determining the molecularity of silane addition reactions.[12] Observation of only the noncrossover products (those incorporating Et_3Si with D or incorporating Pr_3Si with H) illustrates that the mechanism involves addition of the R_3Si unit and the H/D unit from a single molecule of silane into a single molecule of product. Alternatively, observation of the above two compounds in combination with crossover products (those incorporating Et_3Si with H or incorporating Pr_3Si with D) illustrates that the R_3Si unit and H/D unit must come from two different molecules of silane. In interpreting studies of this type, a number of control experiments are necessary. First, it must be demonstrated that the rates of addition of Et_3SiD and Pr_3SiH are comparable. This can be accomplished by evaluating early time points or by judging the ratio of Et_3Si- and Pr_3Si-containing products when an excess of both silanes is employed. Additionally, in the event of crossover products being observed, it must be confirmed that neither the starting silanes nor the silyl-containing products scramble under the reaction conditions. In all crossover experiments described in this study, when a mixture of Et_3SiD and Pr_3SiH is employed, the distribution of the four products is provided as relative percentages, and total crossover is provided as the sum of percentages of the two crossover products. Therefore, reactions that proceed with complete crossover are described here as having 50% total crossover. As the MS analysis of these experiments can be somewhat cumbersome using low-resolution MS methods, a detailed experimental description along with an Excel spreadsheet for simple calculation of crossover percentages is provided as Supporting Information to enable facile evaluation of crossover by standard GC/MS instrumentation.

To summarize the key features of the crossover experiments from the 2004 study, an ynal reductive cyclization proceeded without significant formation of crossover products (generating only products with R = Et, X = D and R = Pr, X = H) using IMes as the ligand, whereas the corresponding reaction with PBu_3 proceeded with substantial crossover product formation (generating all four products with 36% total crossover) (Table 1). The control experiments described above illustrated that the

Table 1. Initial Crossover Data Comparing IMes and PBu_3 as Ligands

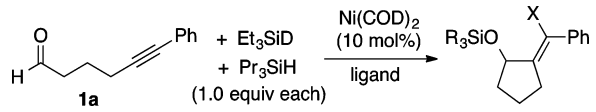

entry	ligand	R = Et, X = H	R = Et, X = D	R = Pr, X = H	R = Pr, X = D	total crossover (%)
1	IMes	<2	55	41	<2	<4
2	PBu_3	22	37	27	14	36

crossover observed with PBu_3 as the ligand was derived from kinetic selectivities during coupling, and not through a scrambling pathway of the starting silanes or final products. The corresponding intermolecular addition of benzaldehyde and phenylpropyne proceeded without crossover utilizing IMes as the ligand, but the PBu_3-promoted intermolecular process was not efficient, thus precluding its analysis in that study.

To explain the crossover observed in the intramolecular couplings employing PBu_3 and organosilanes, it was originally proposed that phosphines and NHC ligands likely proceed via different mechanisms.[5c] The absence of crossover in NHC-ligated systems was consistent with the metallacycle mechanism (Scheme 1), whereas with phosphines, an alternate mechanism might involve generation of a nickel hydride or nickel silyl species, related to the types of species well established in work from Martin,[11] as the active catalyst. Addition of a nickel hydride or silyl species to the ynal, followed by a σ-bond metathesis reaction with the silane, would allow crossover products to be observed. However, the more recent theoretical studies,[9] kinetic analyses,[10] and in situ IR studies[10] cast doubt on these possibilities. While these more recent mechanistic analyses all point to a metallacycle mechanism of the type depicted above, the 2004 crossover study was seemingly inconsistent with the involvement of the metallacycle mechanism (Scheme 1) for the phosphine-promoted pathway.

In this study, we describe an exhaustive evaluation of crossover experiments with a phosphine ligand (PCy_3) that exhibits crossover product formation in some cases while maintaining a broad substrate scope. New insights are provided into the characteristics of ligands, substrates, and reaction conditions that promote crossover in silane-mediated reductive couplings of aldehydes and alkynes. On the basis of these data, a theoretical study was undertaken which provides a modified mechanistic proposal that explains the crossover effects and is consistent with recently described mechanistic analyses.

RESULTS AND DISCUSSION

Crossover Studies. In the initial evaluation of silane crossover experiments, significant crossover was observed in experiments involving five-membered ring cyclizations of ynal **1a** using a catalyst generated from $Ni(COD)_2$ (10 mol %) and PBu_3 (20 mol %). Due to the limited scope of PBu_3-promoted couplings, extensive variation of the ynal substrate was not possible. However, more recent mechanistic studies illustrated

dx.doi.org/10.1021/ja508909u | J. Am. Chem. Soc. 2014, 136, 17495–17504

Table 2. Impact of Ligand Size on Crossover

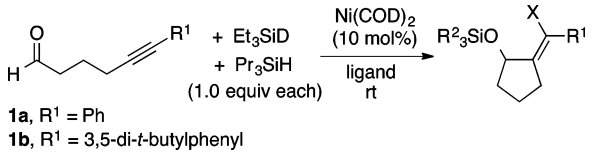

entry	ynal	ligand	R^2 = Et, X = H	R^2 = Et, X = D	R^2 = Pr, X = H	R^2 = Pr, X = D	total crossover (%)
1	**1a**	PBu_3	22	37	27	14	36
2	**1a**	PCy_3	6	55	35	4	10
3	**1b**	PBu_3	26	34	25	15	41
4	**1b**	PCy_3	4	61	31	4	8

that PCy_3 performs as a much more versatile ligand in aldehyde−alkyne reductive couplings with silane reducing agents. On the basis of this finding, an extensive study of crossover effects was undertaken to evaluate the impacts of phosphine sterics, ring size formed, molecularity (inter vs intra), alkyne sterics, temperature, silane concentration, and catalyst loading. In the cases where crossover was observed, recovered silane was analyzed to confirm that scrambling of the silanes had not occurred. In all cases the recovered silane was unchanged. All crossover experiments proceeded with good conversion. Procedures with isolated yields, following the crossover general procedure, are provided for the preparation of all authentic standards in the Supporting Information.

The role of phosphine structure was only studied to a limited extent since most classes of phosphines are inefficient across a broad range of couplings. However, as a benchmark to compare previously reported data using PBu_3 with new data using the more versatile PCy_3 ligand, five-membered cyclizations of two representative ynals were examined (Table 2). With both substrates **1a** and **1b**, more extensive crossover was observed when PBu_3 was employed, while the formation of crossover products with both ligands was minimally impacted as the steric influence of the alkyne substituent was increased. With most of the reaction variables studied below, PBu_3-promoted couplings were inefficient, so data will only be presented with PCy_3 in the evaluation of variations of substrates and reaction conditions. As previously reported, all intermolecular and intramolecular couplings examined with the *N*-heterocyclic carbene ligand IMes proceeded without significant formation of the crossover products, as the examples depicted below illustrate.

Variations in the size of the formed ring and intermolecular couplings were next examined using $Ni(COD)_2$ (10 mol %) and PCy_3 (20 mol %) at rt (Table 3). While the extent of crossover was relatively small in five-membered ring cyclizations, there was a subtle but consistent trend toward diminishing crossover as ring size increases. In the formation of a seven-membered ring, essentially no crossover was observed. In an intermolecular coupling of benzaldehyde and phenylpropyne, crossover was also not observed.

The steric features surrounding the alkyne were next considered (Table 4). In intramolecular couplings, there was a clear trend from terminal alkynes to highly hindered internal alkynes showing that increased sterics diminishes crossover. A comparison of a simple phenyl substituent on the alkyne terminus compared with a 3,5-di-*tert*-butylphenyl substituent illustrated that the trend is maintained even with little variation in electronic bias. The influence of the alkyne steric bulk was also seen in intermolecular reductive couplings, wherein increasing sterics of the distal substituent (R^4 = Me, Et, or Ph) leads to diminished formation of crossover products.

Table 3. Impact of Ring Size and Molecularity on Crossover

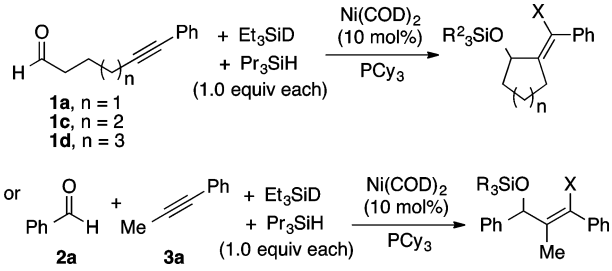

entry	ynal	R = Et, X = H	R = Et, X = D	R = Pr, X = H	R = Pr, X = D	total crossover (%)
1	**1a**	6	55	35	4	10
2	**1c**	5	52	39	4	9
3	**1d**	<1	57	41	<1	<2
4	**2a**/**3a**	<1	59	39	<1	<2

Table 4. Impact of Alkyne Sterics on Crossover

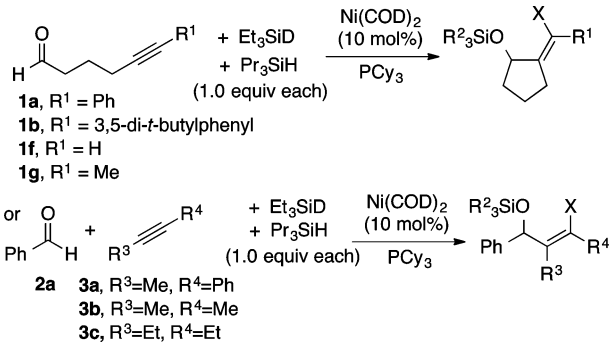

entry	ynal	R^2 = Et, X = H	R^2 = Et, X = D	R^2 = Pr, X = H	R^2 = Pr, X = D	total crossover (%)
1	**1f**	22	30	32	16	38
2	**1g**	19	35	27	19	38
3	**1a**	6	55	35	4	10
4	**1b**	4	61	31	4	8
5	**2a**/**3b**	10	47	37	6	16
6	**2a**/**3c**	5	56	47	2	7
7	**2a**/**3a**	<1	59	39	<1	<2

Variations in temperature led to substantial changes in crossover, with the formation of crossover products increasing as the temperature was lowered (Table 5). With substrates **1a** and **1c** that lead to five- or six-membered ring closure, the small extent of crossover seen at rt was substantially increased as the temperature was lowered. Substrates that show no significant crossover at rt, such as intermolecular combinations (**2a** with

dx.doi.org/10.1021/ja508909u | J. Am. Chem. Soc. 2014, 136, 17495−17504

Table 5. Impact of Temperature on Crossover

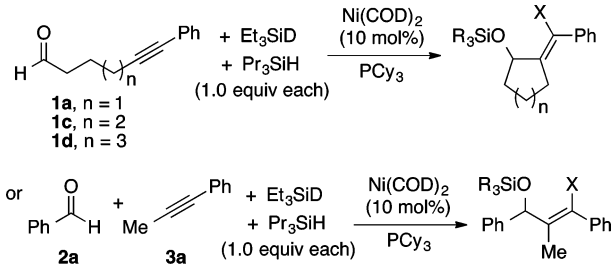

entry	ynal	temp (°C)	R = Et, X = H	R = Et, X = D	R = Pr, X = H	R = Pr, X = D	total crossover (%)
1	**1a**	−25	26	36	24	24	50
2	**1a**	0	7	58	40	5	12
3	**1a**	25	6	55	35	4	10
4	**1a**	45	4	55	37	4	8
5	**1c**	−25	22	34	23	21	43
6	**1c**	25	5	52	39	4	9
7	**1d**	−25	10	52	33	5	15
8	**1d**	25	<1	57	41	<1	<2
9	**2a/3a**	−25	6	46	42	6	12
10	**2a/3a**	25	<1	59	39	<1	<2

3a) and seven-membered ring closures (**1d**), display significant levels of crossover at −25 °C. The observed trends in the formation of crossover show a direct relationship with the temperature, supporting an equilibration between competing pathways.

An increase in crossover was observed as the silane concentration increased (Table 6). Finally, variation in catalyst loading introduced a minimal impact on crossover in experiments ranging from 5 to 20 mol % nickel, in both intra- and intermolecular couplings (Table 7).

In competition experiments employing mixtures of Et_3SiD and Pr_3SiH, several clear trends thus emerge. The changes that lead to the most significant increase in crossover products include a decrease in ligand size, a decrease in alkyne substituent size, the formation of entropically favored ring sizes, and lower reaction temperature. A smaller contribution from silane concentration also plays a minor role, whereas the concentration of catalyst displays essentially no effect. On the basis of these outcomes, a computational evaluation of possible mechanisms was undertaken to further investigate the origin of these effects.

Computational Analysis. As part of a recent study from Houk and Montgomery on the control of regiochemistry in silane-mediated aldehyde−alkyne reductive couplings,[9c] a complete energy profile of a model reaction employing an *N*-heterocyclic carbene ligand with acetaldehyde and 2-butyne as substrates was described. In this sequence, the lowest energy pathway was found to involve oxidative cyclization of Ni(0) π-complex **4** to Ni(II) metallacycle **5** as the rate- and regioselectivity-determining step of the process (Scheme 3, monomer pathway). σ-Bond metathesis with silane affords nickel hydride intermediate **6**, which undergoes reductive elimination to afford product. In a mechanism of this type, no crossover is expected, and this is consistent with experimental observations since NHC ligands do not provide crossover products with any substrates examined.

To evaluate the origin of silane crossover in phosphine-promoted ynal cyclization pathways, we have now computationally evaluated the cyclization of ynal **1g** to product **10** (Scheme 4). The mechanisms of the cyclization were calculated with density functional theory.[13] The geometries were optimized with B3LYP[14] and a mixed basis set of LANL2DZ for nickel and 6-31G(d) for other atoms. Single-point energies were determined with M06[15] and a basis set of SDD for nickel and 6-311+G(d,p) for other atoms. These are the same levels of methods as those we used in the recent computational study of regioselectivity of the intermolecular reductive coupling reaction.[16] The PMe_3 ligand and Me_3SiH were employed in the calculations (see later for computations on the effects of the ligand). The potential energy profiles of the oxidative addition and the σ-bond metathesis steps involving the monomeric and dimeric metallacycles are shown in Figure 1. The free energies and enthalpies are given with respect to the Ni−ynal π-complex **11**.

Oxidative cyclization of the alkyne and aldehyde gives a five-membered metallacycle, **12**. This step (TS1) requires 26.4 kcal/mol in terms of Gibbs free energy and is the rate-determining step in the catalytic cycle. Upon coordination with a trimethylsilane molecule, complex **13** is formed, in which the Ni−H and O−Si distances are 1.83 and 3.01 Å, respectively (Figure 2). The σ-bond metathesis transition state TS2 involves a four-coordinated square planar Ni. The H and Si atoms in the

Table 6. Impact of Silane Concentration on Crossover

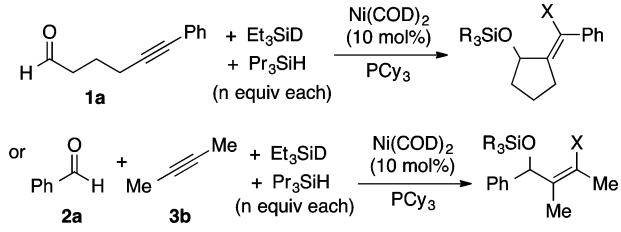

entry	ynal	silane concn (equiv)	R = Et, X = H	R = Et, X = D	R = Pr, X = H	R = Pr, X = D	total crossover (%)
1	**1a**	1	6	55	35	4	10
2	**1a**	2	14	52	26	9	23
3	**1a**	3	17	53	20	10	27
4	**1a**	4	21	54	16	9	30
5	**2a/3b**	1	10	47	37	6	16
6	**2a/3b**	2	12	52	28	8	20
7	**2a/3b**	8	20	49	21	10	30

dx.doi.org/10.1021/ja508909u | J. Am. Chem. Soc. 2014, 136, 17495−17504

Table 7. Impact of Catalyst Concentration on Crossover

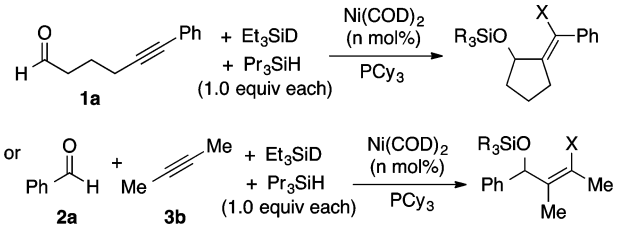

entry	ynal	[Ni(0)] (mol %)	R = Et, X = H	R = Et, X = D	R = Pr, X = H	R = Pr, X = D	total crossover (%)
1	**1a**	10	6	55	35	4	10
2	**1a**	20	7	54	34	5	12
3	**2a**/**3b**	5	8	50	36	6	14
4	**2a**/**3b**	10	10	47	37	6	16
5	**2a**/**3b**	20	10	47	37	6	16

Scheme 3. Mechanistic Pathway Involving Monomeric and Dimeric Metallacyclic Intermediates

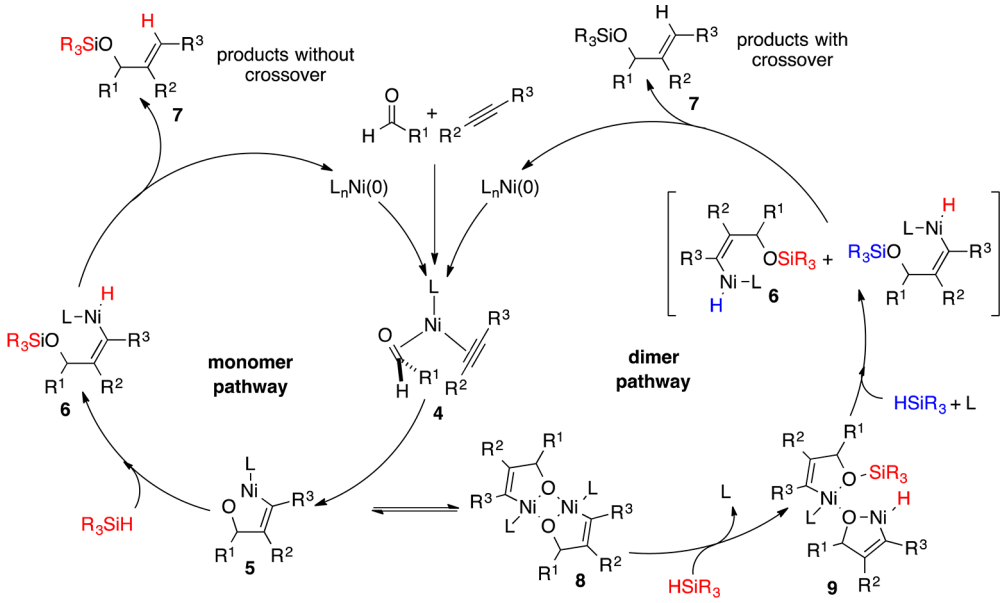

Scheme 4. Model Cyclization for Computational Studies

silane are both in the same plane as the metallacycle and the phosphine. A nickel(II) hydride intermediate, **14**, is formed after the σ-bond metathesis. Complex **14** undergoes facile reductive elimination (TS3) to form product complex **15**, which then undergoes ligand exchange to regenerate reactant complex **11**.[17]

Upon consideration of the dimeric form of the proposed metallacycle, which had been isolated and characterized by Ogoshi (Scheme 2),[8] a new possible pathway emerged as a possible candidate that might be consistent with crossover results, theoretical evaluations, kinetic studies, and in situ IR analyses (Scheme 3). Rather than direct participation of a monomeric metallacycle species, **5**, in the silane-mediated σ-bond metathesis reaction to afford products without crossover, dimerization of **5** to structure **8** could ultimately lead to products with crossover. A likely sequence for the dimer pathway involves ligand exchange in **8**, followed by two sequential σ-bond metathesis reactions to provide intermediate **6**, which would be formed with crossover of the silane mixture employed via the involvement of **9** following the first addition of silane. The conversion of structure **9** to noncrossover products is possible through pathways involving silyl migration. The crossover analysis cannot distinguish between noncrossover products derived from the monomer pathway vs those derived from the dimer pathway accompanied by internal silyl migration. Under some sets of conditions (i.e., Table 5, entry 1), crossover pathways dominate, suggesting that the manifold leading to crossover can proceed without internal silyl migration in some instances. An evaluation of alternative pathways for the σ-bond metathesis step in the dimer-initiated sequence is provided in the Supporting Information.

The initial σ-bond metathesis step in the dimeric pathway for the **1g** to **10** conversion was evaluated computationally (shown in green in Figure 1). Optimized geometries of selected structures in the dimeric pathway are shown in Figure 2b. The formation of metallacycle dimer **17** from the monomer **12** is highly exergonic by 20.2 kcal/mol.[18,19] The dimerization occurs via a van der Waals complex, **16**, which is 4.4 kcal/mol more stable than the monomer metallacycle **12**. The dimerization transition state TS4 requires a low barrier with respect to the

dx.doi.org/10.1021/ja508909u | J. Am. Chem. Soc. 2014, 136, 17495−17504

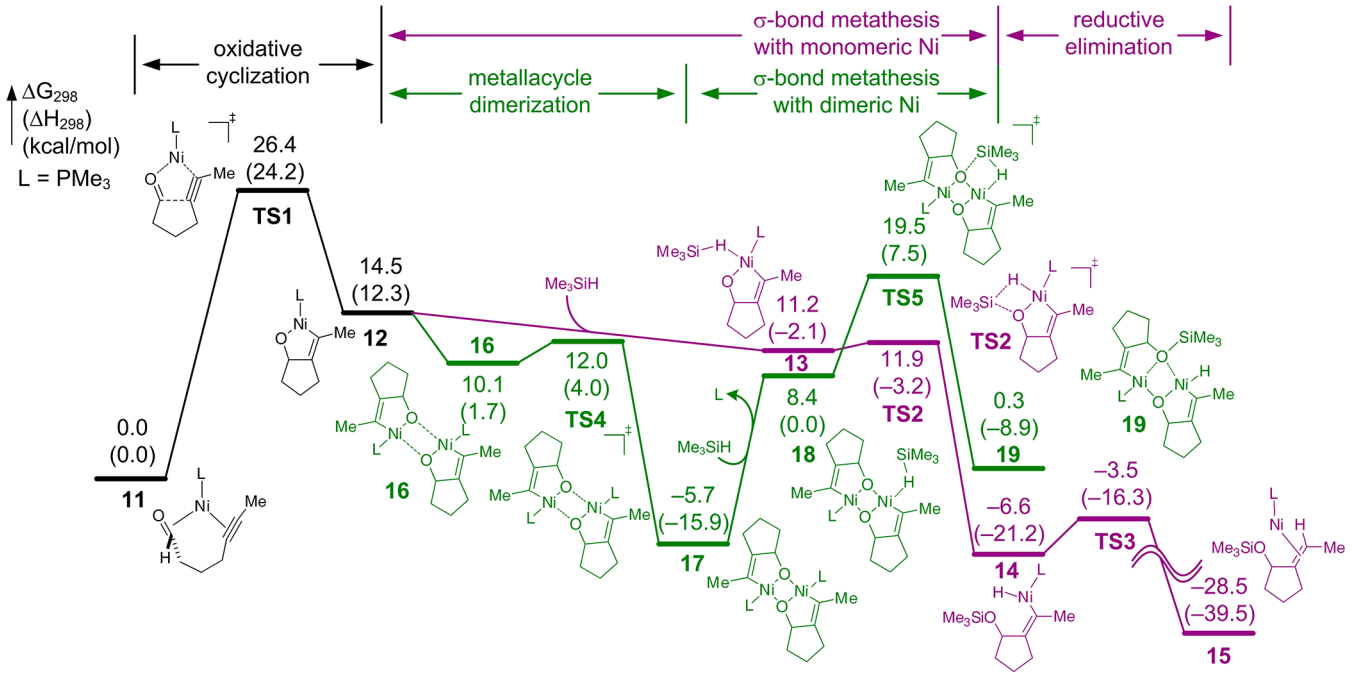

Figure 1. Potential energy surfaces of the monomeric and dimeric pathways (shown in purple and green, respectively) calculated with M06/SDD-6-311+G(d,p)//B3LYP/LANL2DZ-6-31G(d).

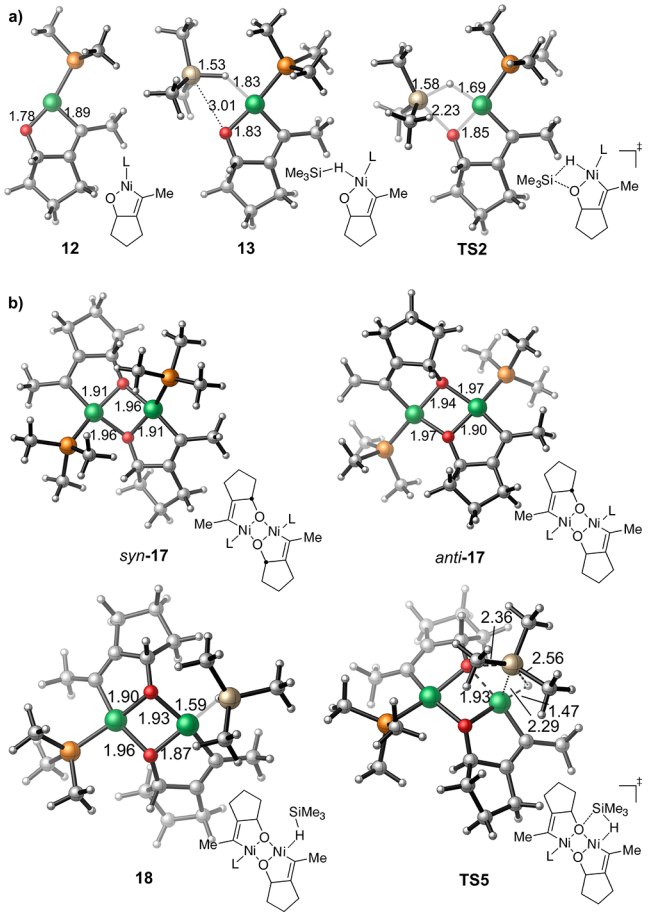

Figure 2. Optimized geometries of intermediates and transition states in the (a) monomeric and (b) dimeric σ-bond metathesis pathways.

van der Waals complex **16**. The intermolecular Ni–O distances decrease from 4.15 Å in the van der Waals complex **16** and 3.62 Å in TS4 to only 1.96 Å in the metallacycle dimer **17**, indicative of strong Ni–O interactions. In comparison, the *intra*molecular Ni–O bonds in **17** are only slightly shorter (1.91 Å). In the dimer complex **17**, although the 16 e$^-$ Ni prefers square planar geometry, the PMe_3 ligands are bent out of the plane to avoid steric repulsions. This presumably promotes the dissociative ligand exchange which replaces a PMe_3 ligand with Me_3SiH to form complex **18**. Due to similar steric constraints, the Si in the σ-bond metathesis transition state TS5 is not coplanar with the metallacycle. The energy required for ligand exchange (**17** → **18**) and the more crowded steric environment in TS5 than in TS2 lead to a higher barrier for σ-bond metathesis in the dimeric pathway than that in the monomeric pathway.[20]

The computed potential energy surfaces indicated that, after the formation of metallacycle **12**, the formation of dimeric intermediate **17** and the monomeric σ-bond metathesis via TS2 both require very low barriers and are highly exothermic. Thus, the exact ratio between these pathways is expected to be affected by nonstatistical dynamic effects.[21] Once the dimer **17** is formed, the complex may undergo dimeric σ-bond metathesis via TS5 to the crossover products or dissociate to **12** and then undergo monomeric σ-bond metathesis via TS2. Calculations indicated the dimeric process (**17** → TS5) requires a 5.0 kcal/mol higher free energy barrier than the monomeric process (**17** → **12** → TS2). Considering the error range of DFT calculations on these challenging species, these results suggest the dimeric and monomeric pathways are competing at room temperature.

To investigate the effects of the ligand and substituents on crossover, we calculated the dissociation energy of the dimeric metallacyclic intermediate **17** ($\Delta G_{17\rightarrow 12}$) and the barrier of σ-bond metathesis from the dimeric intermediate ($\Delta G^{\ddagger}_{17\rightarrow TS5}$) for the reactions of ynal **1g** with different phosphine and NHC ligands (Table 8). The metallacyclic dimer with the bulkier P(*i*-Pr)$_3$ ligand (entry 2) is much easier to dissociate to the monomeric metallacycle **12** than the PMe_3-ligated complex,

dx.doi.org/10.1021/ja508909u | J. Am. Chem. Soc. 2014, 136, 17495–17504

Table 8. Free Energies of Dissociation of Dimeric Metallacyclic Intermediate 17 To Regenerate Monomer 12 ($\Delta G_{17\rightarrow12}$) and Activation Free Energies via a Dimeric σ-Bond Metathesis Pathway ($\Delta G^{\ddagger}_{17\rightarrow TS5}$) in the Reaction of Ynals 1g and 1a with Different Ligands[a]

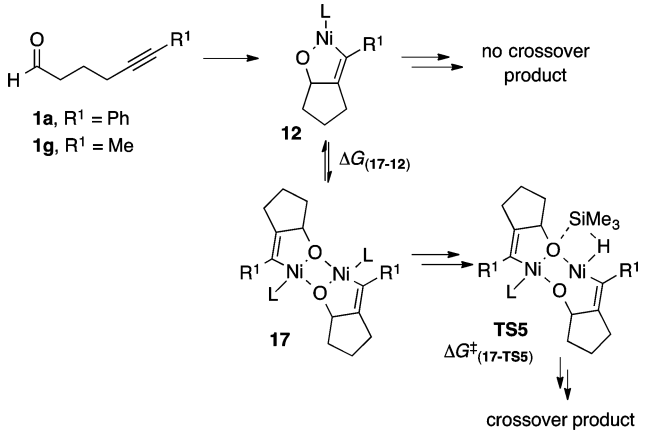

entry	ligand	ynal	$\Delta G_{17\rightarrow12}$	$\Delta G^{\ddagger}_{17\rightarrow TS5}$
1	PMe_3	**1g**	20.3	25.9
2	$P(i\text{-}Pr)_3$	**1g**	15.2	24.2
3	IPh	**1g**	23.7	44.9
4	IMes	**1g**	14.0	36.1
5	PMe_3	**1a**	22.3	31.8

[a]Energies are in kilocalories per mole and with respect to **17**.

while the size of the phosphine ligand has small effects on the barrier for dimeric σ-bond metathesis. Thus, bulkier phosphine ligands are expected to promote the monomeric pathway, leading to lower crossover ratios (see Table 2 for the experimental observation of the effects of the ligand size). Calculations with a small model NHC ligand (IPh) indicated a very high barrier for dimeric σ-bond metathesis (entry 3). The strong coordination of NHC to the metal makes the ligand exchange step (**17** → **18**) highly unfavorable compared to that with phosphine ligands. In addition, the dimer dissociation is much more facile with bulkier NHCs, e.g., IMes (entry 4). In work from Ogoshi, structural evaluation of nickel–NHC metallacycles derived from cyclopropyl ring-opening provide a clear experimental precedent that the monomer/dimer equilibrium is highly sensitive to the steric environment of the substrate.[8c] In summary, strong coordination to the metal and the steric bulk of NHC ligands substantially raise the barrier of the dimeric pathway and promote dissociation to the monomeric metallacycle. This is consistent with the absence of crossover products observed in the NHC-ligated systems (see Table 1).

We also investigated the reaction of ynal **1a** with a terminal phenyl group (entry 5). Increasing the size of the R^1 group from Me to Ph has small effects on the stability of the dimer complex, while it noticeably increases the barrier for dimeric σ-bond metathesis. This is due to steric repulsions between R^1 and $SiMe_3$ groups in TS5 (see the Supporting Information for the optimized geometry of the transition state). This is again consistent with the experimentally observed alkyne steric effects (see Table 4).

Dimer Evaluation. On the basis of the above computational evaluation, we envisioned that the previously reported dimeric metallacycle reported from Ogoshi (Scheme 2)[8] would be interesting to examine in reactions with silanes, especially those with a ligand–substrate structure combination relevant to crossover studies.[22] It should be noted that reductive coupling reactions that proceed with extensive crossover typically are less efficient than protocols that proceed without crossover. We interpret this observation as arising from the thermodynamic stability of dimeric metallacycles, leading to slower catalytic turnovers. This analysis is consistent with the observation that the most effective catalyst systems, such as those involving bulky NHC ligands, proceed without observed crossover. Therefore, a metallacycle presynthesized as the dimer would likely show reduced reactivity in comparison to the most effective catalytic protocols.

To explore the stoichiometric behavior of the Ogoshi metallacycle **20**, this purple crystalline material was used to prepare a 0.01 M solution in THF, and crossover experiments were conducted with 10 equiv each of Et_3SiD and Pr_3SiH (Scheme 5A). While conversions were low, the expected

Scheme 5. Reactivity of a Dimeric Metallacycle with Trialkylsilanes

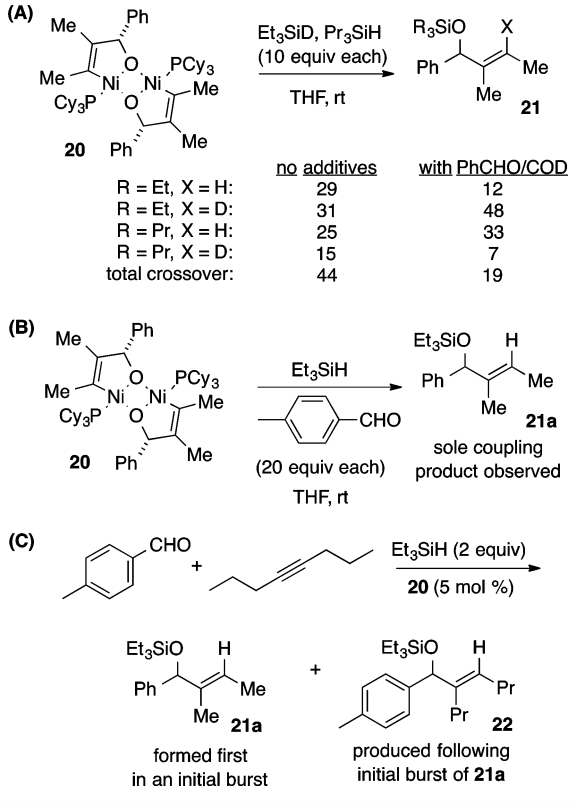

product **21** was obtained with 44% total crossover, which exceeds that seen in a typical catalytic experiment. Repeating the experiment in the presence of benzaldehyde and 1,5-cyclooctadiene improved the reaction efficiency, and the total crossover decreased to 19%, which is very close to that observed in a standard catalytic crossover experiment (entries 5 and 6, Table 6).[23] These results are consistent with crossover resulting from the dimer, whereas benzaldehyde may stabilize coordinatively unsaturated intermediates that allow the dimer to more efficiently access the monomeric metallacycle.

To gauge whether benzaldehyde promotes metallacycle cleavage back to aldehyde and alkyne, an experiment was conducted with the addition of *p*-tolualdehyde and triethylsilane to a THF solution of **20** (Scheme 5B). This experiment

dx.doi.org/10.1021/ja508909u | J. Am. Chem. Soc. 2014, 136, 17495–17504

afforded only benzaldehyde-derived product **21a**, illustrating that the dimer **20** is chemically competent and that metallacycle cleavage to free aldehyde and alkyne does not occur under catalytically relevant conditions.[24] This is consistent with the computed energy profile shown in Figure 1, which indicated the monomeric and dimeric σ-bond metathesis pathways both require a lower barrier than the reverse reaction to cleave the metallacycle via TS1. Finally, to probe the kinetic competence of dimer **20**, the reductive coupling of *p*-tolualdehyde, 4-octyne, and triethylsilane was conducted using **20** as the catalyst in 5 mol % concentration (Scheme 5C). While the reaction proceeded efficiently, the earliest time points displayed an initial burst of product **21a**, followed by the appearance of **22**. This experiment illustrates that the dimer conversion to product is faster than the rate of the complete catalytic cycle starting from aldehyde and alkyne.[25]

Evaluation of Crossover Trends. Considering the proposed dimer pathway within the context of the theoretical analysis and studies of the independently prepared dimer, it is instructive to consider the observed crossover data (Tables 2−7) compared with the proposed mechanistic pathway (Scheme 3 and Figure 1). Increasing either the ligand size (Table 2) or alkyne sterics (Table 4) results in a substantially decreased level of crossover. These changes have a major influence on the mechanistic path followed, and the influence of sterics on the monomer/dimer equilibrium and on the activation barrier for dimer consumption has been elucidated through a computational evaluation (Table 8). The temperature effects (Table 5) are also substantial, and the effect originates from influencing the K_{eq} for the monomer/dimer equilibrium. The dimeric pathway becomes more favorable at low temperature since the dimer is enthalpically favored but entropically disfavored. The ring size and molecularity (Table 3) undoubtedly influence the rate of formation of the initially produced monomeric metallacycle. Less favorable ring sizes that diminish the rate of metallacycle formation should disfavor the involvement of a pathway that involves metallacycle dimerization. Additionally, smaller ring sizes will lead to less steric repulsion with the ligand during dimer assembly.

The extent of crossover increases as the silane concentration increases (Table 6). Consumption of both the monomer and dimer requires silane addition; however, the barrier for silane addition to the monomer (TS2, Figure 1) is extremely small, whereas the barrier for silane addition to the dimer (TS5, Figure 1) is substantial. Therefore, the increase in silane concentration would be expected to more dramatically increase the rate of dimer conversion to product compared with the minimal impact of the silane concentration on conversion of monomer to product, consistent with the observations. The very small influence of the catalyst concentration (Table 7) is perhaps surprising given that the monomer−dimer equilibrium would shift toward the dimer at higher catalyst concentration. However, all crossover experiments were performed with a constant 1:2 metal:ligand ratio at constant volume. Therefore, the concentration of free COD and phosphine in solution increases as the active catalyst concentration increases, and these simultaneous changes may affect both the monomer−dimer equilibrium (**12** to **17**, Figure 1) and the ligand dissociation required for the dimer conversion to product (**17** to **18**, Figure 1). The experimental parameters that most impact the extent of crossover, namely, ligand and substrate sterics, ring size, temperature, and silane concentration, are all readily explained by the proposed dual involvement of monomer and dimer pathways.

SUMMARY AND CONCLUSIONS

In summary, the involvement of a novel dimeric pathway has been evaluated in nickel-catalyzed silane-mediated reductive couplings of ynals. The analysis of silane crossover (using Et_3SiD and Pr_3SiH) was extensively studied across a range of ligand and substrate variations, including various ring sizes and intermolecular versions. The effects of temperature variation and the concentration of silane and catalyst were also examined. A computational study comparing monomeric and dimeric pathways, both involving initial formation of a metallacycle from oxidative cyclization of a nickel(0) aldehyde−alkyne π-complex, provides evidence for the competitive nature of the two pathways. Identification of the key steps that determine the predominance of the monomeric or dimeric pathways is supported by the silane crossover experiments. The independent synthesis of a dimeric metallacycle confirmed that its conversion to product upon treatment with silane proceeds predominantly through a crossover pathway.

A general and useful trend that can be seen from these studies is that the most efficient protocols, proceeding in high yields with the broadest range of substrates, correlate to the reaction conditions that minimize crossover. We attribute this effect to the considerable stability of the metallacycle dimers of structure type **8** (Scheme 3). Protocols that proceed predominantly via the monomer pathway, such as silane-based procedures employing bulky NHC ligands[5c,d] or borane-based procedures,[4] which would likely impede metallacycle dimerization due to coordination of the borane to the metallacycle oxygen, are the most robust methods across a range of substrate combinations. The analysis reported herein of the dimeric pathways and their influence on catalytic cycle efficiency can thus serve as a guide to predicting optimum catalyst−reductant combinations as well as identifying substrate combinations that may proceed inefficiently. The silane crossover technique provides a simple and rapid analysis method for evaluating the complex mechanistic trends highlighted in this study.

ASSOCIATED CONTENT

Supporting Information

Detailed experimental procedures and computational methods and Excel spreadsheet for the calculation of the ratio of two compounds that differ only in isotope incorporation. This material is available free of charge via the Internet at http://pubs.acs.org.

AUTHOR INFORMATION

Corresponding Authors

houk@chem.ucla.edu
jmontg@umich.edu

Present Addresses

[‖]P.L.: Department of Chemistry, University of Pittsburgh, 219 Parkman Ave., Pittsburgh, PA 15260.
[⊥]R.D.B.: Department of Chemistry, University of California at Merced, 5200 N. Lake Rd., Merced, CA 95343.

Author Contributions

[§]M.T.H. and P.L. contributed equally to this work.

Notes

The authors declare no competing financial interest.

■ ACKNOWLEDGMENTS

We are grateful to the National Institutes of Health (Grant GM57014, J.M.) and the National Science Foundation (Grant CHE-1059084, K.N.H.) for financial support. Professor Anne McNeil is thanked for helpful suggestions.

■ REFERENCES

(1) For reviews on nickel-catalyzed reductive coupling, see: (a) Montgomery, J. Organonickel Chemistry. In *Organometallics in Synthesis*, 4th manual; Lipshutz, B. H., Ed.; Wiley: Hoboken, NJ, 2013; pp 319−428. (b) Montgomery, J. *Angew. Chem., Int. Ed.* **2004**, *43*, 3890−3908. (c) Tasker, S. Z.; Standley, E. A.; Jamison, T. F. *Nature* **2014**, *509*, 299−309. (d) Moslin, R. M.; Miller-Moslin, K.; Jamison, T. F. *Chem. Commun.* **2007**, 4441−4449. (e) Montgomery, J.; Sormunen, G. J. In *Metal Catalyzed Reductive C−C Bond Formation: A Departure from Preformed Organometallic Reagents*; Krische, M. J., Ed.; Springer: Berlin, 2007; Vol. *279*, pp 1−23. (f) Montgomery, J. *Acc. Chem. Res.* **2000**, *33*, 467−473. (g) Tanaka, K.; Tajima, Y. *Eur. J. Org. Chem.* **2012**, 3715−3725.

(2) For examples of related reductive couplings with other metals, see: (a) Kablaoui, N. M.; Buchwald, S. L. *J. Am. Chem. Soc.* **1995**, *117*, 6785−6786. (b) Ojima, I.; Tzamarioudaki, M.; Tsai, C. Y. *J. Am. Chem. Soc.* **1994**, *116*, 3643−3644. (c) Jang, H. Y.; Krische, M. J. *Acc. Chem. Res.* **2004**, *37*, 653−661. (d) Bower, J. F.; Kim, I. S.; Patman, R. L.; Krische, M. J. *Angew. Chem., Int. Ed.* **2009**, *48*, 34−46. (e) Ngai, M. Y.; Kong, J. R.; Krische, M. J. *J. Org. Chem.* **2007**, *72*, 1063−1072. (f) Reichard, H. A.; McLaughlin, M.; Chen, M. Z.; Micalizio, G. C. *Eur. J. Org. Chem.* **2010**, 391−409. (g) Bahadoor, A. B.; Flyer, A.; Micalizio, G. C. *J. Am. Chem. Soc.* **2005**, *127*, 3694−3695.

(3) (a) Montgomery, J.; Oblinger, E.; Savchenko, A. V. *J. Am. Chem. Soc.* **1997**, *119*, 4911−4920. (b) Lozanov, M.; Montgomery, J. *Tetrahedron Lett.* **2001**, *42*, 3259−3261. (c) Qi, X.; Montgomery, J. *J. Org. Chem.* **1999**, *64*, 9310−9313.

(4) (a) Huang, W.-S.; Chan, J.; Jamison, T. F. *Org. Lett.* **2000**, *2*, 4221−4223. (b) Chan, J.; Jamison, T. F. *J. Am. Chem. Soc.* **2003**, *125*, 11514−11515. (c) Colby, E. A.; O'Brien, K. C.; Jamison, T. F. *J. Am. Chem. Soc.* **2004**, *126*, 998−999. (d) Miller, K. M.; Luanphaisarnnont, T.; Molinaro, C.; Jamison, T. F. *J. Am. Chem. Soc.* **2004**, *126*, 4130−4131.

(5) (a) Tang, X.-Q.; Montgomery, J. *J. Am. Chem. Soc.* **1999**, *121*, 6098−6099. (b) Tang, X.-Q.; Montgomery, J. *J. Am. Chem. Soc.* **2000**, *122*, 6950−6954. (c) Mahandru, G. M.; Liu, G.; Montgomery, J. *J. Am. Chem. Soc.* **2004**, *126*, 3698−3699. (d) Malik, H. A.; Sormunen, G. J.; Montgomery, J. *J. Am. Chem. Soc.* **2010**, *132*, 6304−6305.

(6) Chan, J.; Jamison, T. F. *J. Am. Chem. Soc.* **2004**, *126*, 10682−10691.

(7) (a) Colby, E. A.; O'Brien, K. C.; Jamison, T. F. *J. Am. Chem. Soc.* **2004**, *126*, 998−999. (b) Colby, E. A.; O'Brien, K. C.; Jamison, T. F. *J. Am. Chem. Soc.* **2005**, *127*, 4297−4307. (c) Knapp-Reed, B.; Mahandru, G. M.; Montgomery, J. *J. Am. Chem. Soc.* **2005**, *127*, 13156−13157. (d) Shareef, A.-R.; Sherman, D. H.; Montgomery, J. *Chem. Sci.* **2012**, *3*, 892−895. (e) Chrovian, C. C.; Knapp-Reed, B.; Montgomery, J. *Org. Lett.* **2008**, *10*, 811−814.

(8) (a) Ogoshi, S.; Arai, T.; Ohashi, M.; Kurosawa, H. *Chem. Commun.* **2008**, 1347−1349. (b) Ogoshi, S.; Oka, M.; Kurosawa, H. *J. Am. Chem. Soc.* **2004**, *126*, 11802−11803. (c) Tamaki, T.; Nagata, M.; Ohashi, M.; Ogoshi, S. *Chem.—Eur. J.* **2009**, *15*, 10083.

(9) (a) McCarren, P. R.; Liu, P.; Cheong, P. H. Y.; Jamison, T. F.; Houk, K. N. *J. Am. Chem. Soc.* **2009**, *131*, 6654−6655. (b) Liu, P.; McCarren, P.; Cheong, P. H. Y.; Jamison, T. F.; Houk, K. N. *J. Am. Chem. Soc.* **2010**, *132*, 2050−2057. (c) Liu, P.; Montgomery, J.; Houk, K. N. *J. Am. Chem. Soc.* **2011**, *133*, 6956−6959. (d) For a computational study on the mechanism of Ni-catalyzed alkyne−*enone* reductive coupling reactions with $ZnMe_2$ reductant in a ligand-free system, see: Hratchian, H. P.; Chowdhury, S. K.; Gutierrez-Garcia, V. M.; Amarasinghe, K. K. D.; Heeg, M. J.; Schlegel, H. B.; Montgomery, J. *Organometallics* **2004**, *23*, 4636−4646. For computational studies on *rhodium*-catalyzed reductive coupling reactions, see: (e) Williams, V. M.; Kong, J.-R.; Ko, B.-J.; Mantri, Y.; Brodbelt, J. S.; Baik, M.-H.; Krische, M. J. *J. Am. Chem. Soc.* **2009**, *131*, 16054−16062. (f) Liu, P.; Krische, M. J.; Houk, K. N. *Chem.—Eur. J.* **2011**, *17*, 4021−4029.

(10) Baxter, R. D.; Montgomery, J. *J. Am. Chem. Soc.* **2011**, *133*, 5728−5731.

(11) Work from Martin has illustrated that nickel silyl and nickel hydride intermediates are generated at 100 °C using phosphine catalysts. While such intermediates would be consistent with silane crossover, the generation of the requisite nickel hydride and silyl species does not occur in the temperature range of our studies. See: Cornella, J.; Gómez-Bengoa, E.; Martin, R. *J. Am. Chem. Soc.* **2013**, *135*, 1997−2009.

(12) (a) Trost, B. M.; Ball, Z. T. *J. Am. Chem. Soc.* **2003**, *125*, 30. (b) Takacs, J. M.; Chandramouli, S. *Organometallics* **1990**, *9*, 2877. (c) Parks, D. J.; Blackwell, J. M.; Piers, W. E. *J. Org. Chem.* **2000**, *65*, 3090.

(13) All calculations were performed with Gaussian 09: Frisch, M. J.; Trucks, G. W.; Schlegel, H. B.; Scuseria, G. E.; Robb, M. A.; Cheeseman, J. R.; Scalmani, G.; Barone, V.; Mennucci, B.; Petersson, G. A.; Nakatsuji, H.; Caricato, M.; Li, X.; Hratchian, H. P.; Izmaylov, A. F.; Bloino, J.; Zheng, G.; Sonnenberg, J. L.; Hada, M.; Ehara, M.; Toyota, K.; Fukuda, R.; Hasegawa, J.; Ishida, M.; Nakajima, T.; Honda, Y.; Kitao, O.; Nakai, H.; Vreven, T.; Montgomery, J. A., Jr.; Peralta, J. E.; Ogliaro, F.; Bearpark, M.; Heyd, J. J.; Brothers, E.; Kudin, K. N.; Staroverov, V. N.; Kobayashi, R.; Normand, J.; Raghavachari, K.; Rendell, A.; Burant, J. C.; Iyengar, S. S.; Tomasi, J.; Cossi, M.; Rega, N.; Millam, J. M.; Klene, M.; Knox, J. E.; Cross, J. B.; Bakken, V.; Adamo, C.; Jaramillo, J.; Gomperts, R.; Stratmann, R. E.; Yazyev, O.; Austin, A. J.; Cammi, R.; Pomelli, C.; Ochterski, J. W.; Martin, R. L.; Morokuma, K.; Zakrzewski, V. G.; Voth, G. A.; Salvador, P.; Dannenberg, J. J.; Dapprich, S.; Daniels, A. D.; Farkas, O.; Foresman, J. B.; Ortiz, J. V.; Cioslowski, J.; Fox, D. J. *Gaussian 09*, revision D.01; Gaussian, Inc.: Wallingford, CT, 2009.

(14) (a) Becke, A. D. *J. Chem. Phys.* **1993**, *98*, 5648. (b) Lee, C.; Yang, W.; Parr, R. G. *Phys. Rev. B* **1988**, *37*, 785.

(15) (a) Zhao, Y.; Truhlar, D. G. *Acc. Chem. Res.* **2008**, *41*, 157. (b) Minenkov, Y.; Occhipinti, G.; Jensen, V. R. *J. Phys. Chem. A* **2009**, *113*, 11833.

(16) Test calculations using M06 for geometry optimizations give similar results. See the Supporting Information for details.

(17) The ligand exchange step to liberate product **10** and coordinate with another reactant molecule **1g** to regenerate **11** is exergonic by 15.7 kcal/mol.

(18) This dimerization energy is calculated per mole of the monomeric metallacycle **12**.

(19) Two isomers were located for the metallacycle dimer **17** (Figure 2b): the two hydrogen atoms on the aldehyde carbon may be *syn* or *anti* to each other. The *syn* isomer is 0.3 kcal/mol more stable than the *anti* isomer. Previous studies by Ogoshi indicated the *syn* and *anti* isomers are in equilibrium: see ref 8a.

(20) The second σ-bond metathesis step, which involves addition of another R_3SiH molecule to the intermolecular Ni−O bond in **19**, does not require dissociation of the phosphine ligand, and the transition state is less crowded than TS5. Calculations suggest this process is expected to be more facile than the first σ-bond metathesis (TS5). See the Supporting Information for more details.

(21) (a) Reyes, M. B.; Carpenter, B. K. *J. Am. Chem. Soc.* **2000**, *122*, 10163−10176. (b) Oyola, Y.; Singleton, D. A. *J. Am. Chem. Soc.* **2009**, *131*, 3130−3131. (c) Goldman, L. M.; Glowacki, D. R.; Carpenter, B. K. *J. Am. Chem. Soc.* **2011**, *133*, 5312−5318.

(22) For a recent report describing the catalytic relevance of a dimeric nickel species, see: Stolley, R. M.; Duong, H. A.; Thomas, D. R.; Louie, J. *J. Am. Chem. Soc.* **2012**, *134*, 15154−15162. For other examples of processes that proceed through involvement of bimetallic species, see: (b) Konsler, R. G.; Karl, J.; Jacobsen, E. N. *J. Am. Chem. Soc.* **1998**, *120*, 10780. (c) Schmidbaur, H.; Franke, R. *Inorg. Chim. Acta* **1975**, *13*, 85−89. (d) Fackler, J. P.; Basil, J. D. *Organometallics* **1982**, *1*, 871−873. (e) Basil, J. D.; Murray, H. H.; Fackler, J. P.; Tocher, J.; Mazany, A. M.; Trzcinska-Bancroft, B.; Knachel, H.; Dudis,

D.; Delord, T. J.; Marler, D. O. *J. Am. Chem. Soc.* **1985**, *107*, 6908−6915.
(23) Ogoshi similarly reported that aldehyde addition improved the efficiency of conversions involving organozinc additions; see ref 8a.
(24) For studies probing reversibility of metallacycle formation in aldehyde−diene couplings, see: (a) Park, B. Y.; Montgomery, T. P.; Garza, V. J.; Krische, M. J. *J. Am. Chem. Soc.* **2013**, *135*, 16320−16323. (b) Ogoshi, S.; Tonomori, K.-i.; Oka, M.-a.; Kurosawa, H. *J. Am. Chem. Soc.* **2006**, *128*, 7077−7086.
(25) In nickel-catalyzed enal−alkyne cyclizations, an independently prepared metallacycle was documented to not be kinetically competent in an experiment analogous to Scheme 5C. See ref 9d.